Available online at www.sciencedirect.com
SCIENCE DIRECT
Polyhedron 25 (2006) 1519–1530
POLYHEDRON
www.elsevier.com/locate/poly

Synthetic, crystallographic and electrochemical studies of thienyl-substituted corrole complexes of copper and cobalt

Nilkamal Maiti, Junseong Lee, Seong Jung Kwon, Juhyoun Kwak, Youngkyu Do, David G. Churchill *

Department of Chemistry and School of Molecular Science (BK 21), KAIST, 373-1 Guseong-dong, Yuseong-gu, Daejeon 305-701, Republic of Korea

Received 30 August 2005; accepted 14 October 2005
Available online 29 November 2005

Abstract

The TFA-catalyzed condensation of 5-(thienyl)dipyrromethane with thiophene carboxaldehyde allows for the formation of the thienyl *meso*-substituted 5,10,15-tris(2-thienyl)corrole H_3(T2TC) (**1**) and the 5,10,15-tris(3-thienyl)corrole H_3(T3TC) (**2**). These ligands undergo metalation with copper and cobalt acetate to yield the four respective metallocorroles. Single-crystal X-ray crystallographic solutions for Cu(T2TC) (**3**), Co(T2TC)$(Py)_2$ (**5**) and Co(T3TC)$(Py)_2$ (**6**) have been obtained, confirming the direct pyrrole–pyrrole link and axial pyridine groups in the case of the cobalt structures. Cyclic voltammetry data indicated the 2-thienyl derivatives are more difficult to oxidize when compared to trispentafluorophenyl corroles (TPFC). Both metal complex isomers are comparably stable towards the formation of dinuclear products resulting from intermolecular C–C coupling. Soret bands for both ligands and complexes have been obtained and variable temperature ^{1}H NMR studies (−50–60 °C) for **3** and **4** reveal a fluxional rotational behavior for the three thienyl substituents believed to impart a less electron withdrawing effect on the corrole core, opposed to the TPFC's.

Keywords: Corrole; Cobalt; Copper; Thienyl-substitution; Cyclic voltammetry; Crystal structure

1. Introduction

Corroles are core-modified porphyrins in that they lack one methine group, possess a direct pyrrole–pyrrole bond and provide for a contracted *triv*alent cavity known to stabilize metal ions of higher formal oxidation state (Fig. 1) [1–13]. Metallocorroles are of particular research interest with respect to catalytic activity [3,14–18] and simulating enzymatic oxygen atom transfer type reactions [3,19]. Convenient methodologies for additional functionalization have recently been discovered and previously reported [20–22]. Other intriguing features of metallocorroles include high fluorescent quantum yields [12,23–25], selective interactions with proteins and tumor cells [21,26,27], and substitutions to achieve water solubility [20].

Our aim was to investigate corroles with previously unexplored five-membered substituents and the corresponding copper and cobalt complexes. Previously, β-pyrrole-β-pyrrole coupling (by way of C–C bond formation) in copper and cobalt corrole complexes has been observed for less sterically bulky groups at the *meso* positions [8,11]. Gross and co-workers [8] have reported the synthesis of monomeric copper corrole complexes by using sterically protected 2,6-dichlorophenyl groups compared to pentafluorophenyl groups at the *meso* positions of the corrole but there is still occurrence of C–C coupling that can interfere with the goal of elucidating single site metal-based catalysis pathways. While this report is not the first to report copper corrole complexes that have a reduced tendency to dimerize [28,29], the thiophene substitutions may differently allow for *thienyl–thienyl* coupling, giving polymer-type metal complex networks.

A secondary aim was to explore substitutions of less steric encumbrance, compared to 2,6-dichlorophenyl and

* Corresponding author. Tel.: +82 42 869 2845.
E-mail address: dchurchill@kaist.ac.kr (D.G. Churchill).

0277-5387/$ - see front matter © 2005 Elsevier Ltd. All rights reserved.
doi:10.1016/j.poly.2005.10.016

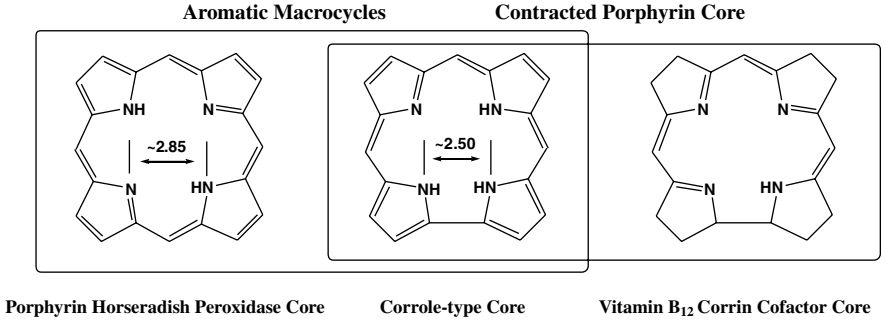

Fig. 1. A comparison of porphyrin derivative metal binding cores.

pentafluorophenyl group substitution at the *meso* positions of the corrole. Metalloporphyrins bearing thienyl substituents on all *meso* groups (tetrathienyl-substituted) have been reported in which the metal is copper [30,31] or cobalt [32]. Thus, studying metallocorroles with thienyl substitution allows us to probe the steric and electronic effects at the metal site [28,33]. Presence of peripheral sulfur groups may furthermore open the possibility for subsequent metal ion binding and allow for supramolecular assemblies.

Thienyl group substituents are comparable to phenyl substitution and are far removed from the electron withdrawing capacity of the pentafluorophenyl group. However, this can be evaluated by electrochemical studies and a consideration of Hammett parameters. We have recently reported the synthesis and crystallographic structures of both 5-(thienyl)dipyrromethane isomers [34]. Thus, herein we describe the synthesis and full characterization of new 5,10,15-tris(thienyl)metallocorroles by techniques that include single-crystal X-ray diffraction, spectroscopy, mass spectrometry, and cyclic voltammetry. Importantly, the molecular structures of 2-thienyl metallocorrole complexes of copper and cobalt, and the 3-thienyl cobalt corrole have been obtained (see Scheme 1).

2. Results and discussion

2.1. Synthesis

Both free base thienyl corroles were prepared from the respective dipyrromethanes and aldehydes using general conditions previously developed for sterically unhindered dipyrromethanes [35]. In particular, the reaction between 5-(2-thienyl)dipyrromethane or 5-(3-thienyl)dipyrromethane [34] and thiophene carboxyaldehyde occurs with the addition of a catalytic amount of TFA; subsequent addition of DDQ gives the green fluorescent 5,10,15-tris(2-thienyl)corrole and 5,10,15-tris(3-thienyl)corrole, respectively (Scheme 1). Both copper complexes **3** and **4** were obtained by the reaction of the corresponding 5,10,15-tris(thienyl)corrole with excess $Cu(OAc)_2 \cdot H_2O$ in pyridine solution at room temperature. This synthetic step is very low yielding in the overall scheme providing ca. 3%

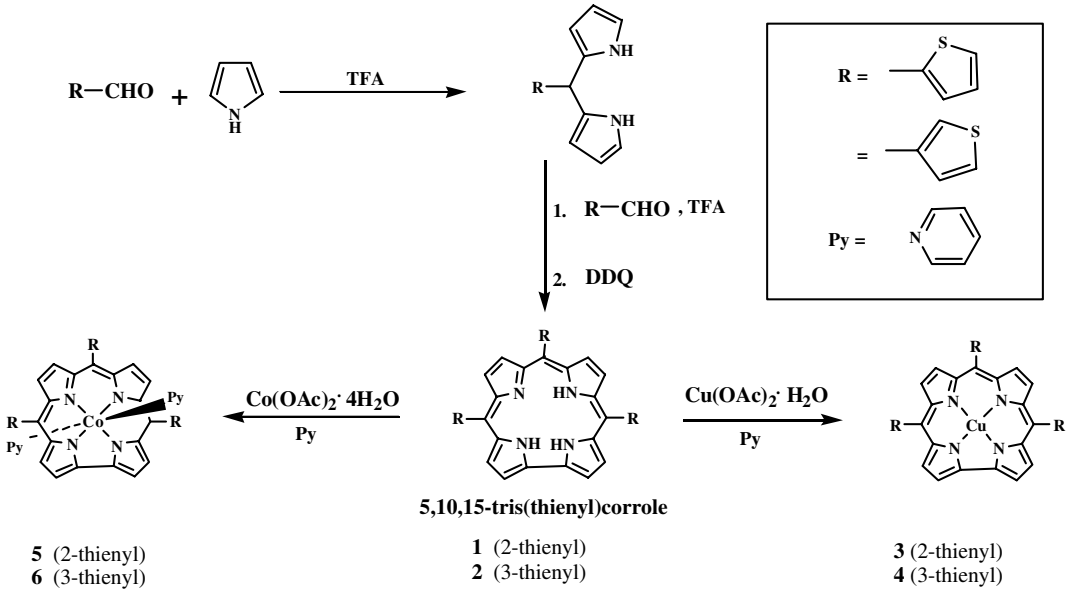

Scheme 1. Preparation of 5,10,15-tris(thienyl)corroles and their corresponding copper complexes and cobalt bis-pyridine complexes.

of free base. The direct synthesis of such corroles from aldehydes and pyrrole was not achievable in our hands.

Metallation occurs rapidly and accompanied by a visible color change. The corresponding reddish-brown copper complexes were obtained within 20 min with yields of ca. 90%. Both cobalt complexes **5** and **6** were obtained by the reaction of the corresponding 5,10,15-tris(thienyl)corrole with excess $Co(OAc)_2 \cdot 4H_2O$ in a refluxing pyridine solution for an overall yield of ca. 90%.

The stability of complexes **3**–**6** are notable in contrast to some related copper and cobalt systems with the electron withdrawing $-C_6F_5$ groups at the three *meso* positions [8,11]. For the copper species, there is no green component in the reaction mixture as in the tris-pentafluorophenyl-substituted corrole reported by Gross and coworkers [8]. The solution containing the copper complexes remains reddish-brown after one week at RT and in the absence of light. This points to an enhanced stability towards C–C coupling compared to the trispentafluorophenyl corroles and has furthered our interest in these derivatives [8,11]. Thus, CV data and diffraction studies have been obtained and are presented and discussed below to attempt to understand the unique properties of thienyl substitution.

2.2. Structural studies

We have conducted single-crystal X-ray diffraction studies of Cu(T2TC) (**3**), Co(T2TC)$(Py)_2$ (**5**) and Co(T2TC)$(Py)_2$ (**6**) (Tables 1 and 2). Complex **3** was found to crystallize in the monoclinic space group $C2/c$ with the cell parameters: $a = 10.374(13)$ Å, $b = 23.21(3)$ Å, $c = 20.625(17)$ Å, $\beta = 95.53(5)°$, $V = 4942(9)$ Å^3, and contained no solvent of crystallization. The cell parameters for the analogous tris-substituted 3-thienyl derivatives **5** and **6** are as follows: (**5**), triclinic, $P\bar{1}$, $a = 11.6509(13)$ Å, $b = 12.4878(14)$ Å, $c = 15.4676(18)$ Å, $\alpha = 98.237(2)°$, $\beta = 105.613(2)°$, $\gamma = 106.376(2)°$, $V = 2020.1(4)$ Å^3; (**6**) triclinic, $P\bar{1}$, $a = 9.705(4)$ Å, $b = 11.745(5)$ Å, $c = 16.401(6)$ Å, $\alpha = 101.298(7)°$, $\beta = 95.059(7)°$, $\gamma = 112.872(7)°$ and $V = 1661.0(11)$ Å^3, $Z = 2$. The solution for **5** and **6** contained two axial pyridine ligands and a benzene solvent of crystallization in the case of **5**. The molecular structures and packing diagrams for compound **3** are provided in Figs. 2 and 3; these diagrams for compounds **5** and **6** are found in Figs. 5–8. The crystallographic data for **3**, **5** and **6** is summarized in Table 3.

Table 1
Selected bond distances and angles in Cu(T2TC) (**3**)

Distances	
Cu–N(3)	1.886(4)
Cu–N(1)	1.888(5)
Cu–N(4)	1.889(4)
Cu–N(2)	1.891(4)
C(1)–C(19)	1.446(7)
Angles	
N(3)–Cu–N(4)	90.76(18)
N(1)–Cu–N(4)	82.60(19)
N(3)–Cu–N(2)	97.46(16)
N(1)–Cu–N(2)	91.18(18)

Table 2
Selected bond distances and angles for Co(T2TC)$(Py)_2$ (**5**) and Co(T3TC)$(Py)_2$ (**6**)

Co(T2TC)(Py_2)		Co(T3TC)(Py_2)	
Co–N(1)	1.861(5)	Co(1)–N(1)	1.866(3)
Co–N(2)	1.894(5)	Co(1)–N(4)	1.871(3)
Co–N(3)	1.898(5)	Co(1)–N(3)	1.892(3)
Co–N(4)	1.863(5)	Co(1)–N(2)	1.904(3)
Co–N(5)	2.004(5)	Co(1)–N(6)	1.998(3)
Co–N(6)	1.981(4)	Co(1)–N(5)	1.998(3)
N(1)–Co–N(4)	82.5(2)	N(1)–Co(1)–N(4)	82.12(13)
N(1)–Co–N(2)	91.5(2)	N(1)–Co(1)–N(3)	173.47(12)
N(4)–Co–N(2)	173.8(2)	N(4)–Co(1)–N(3)	91.41(13)
N(1)–Co–N(3)	173.0(2)	N(1)–Co(1)–N(2)	91.27(12)
N(4)–Co–N(3)	90.5(2)	N(4)–Co(1)–N(2)	173.39(13)
N(2)–Co–N(3)	95.5(2)	N(3)–Co(1)–N(2)	95.20(13)
N(1)–Co–N(6)	90.16(19)	N(1)–Co(1)–N(6)	91.07(13)
N(4)–Co–N(6)	91.79(19)	N(4)–Co(1)–N(6)	89.14(13)
N(2)–Co–N(6)	90.00(19)	N(3)–Co(1)–N(6)	89.69(12)
N(3)–Co–N(6)	89.96(19)	N(2)–Co(1)–N(6)	90.97(12)
N(1)–Co–N(5)	90.8(2)	N(1)–Co(1)–N(5)	88.35(12)
N(4)–Co–N(5)	90.9(2)	N(4)–Co(1)–N(5)	88.26(12)
N(2)–Co–N(5)	87.42(19)	N(3)–Co(1)–N(5)	90.60(12)
N(3)–Co–N(5)	89.4(2)	N(2)–Co(1)–N(5)	91.59(12)
N(6)–Co–N(5)	177.3(2)	N(6)–Co(1)–N(5)	177.39(12)

The *meso* aryl groups are often found approximately normal to the corrole plane. For the thienyl groups, there is a wide range of $C_{pyrrolyl}$–C_{meso}–C_{ipso}–$C_{thienyl}$ dihedral values. For the copper compound, the angles were ca. 26°, 43° and 53° showing great flexibility of the thienyl moiety. Additionally, these angles for the cobalt complex **5** were ca. 52°, 86° and 87° and for **6** were ca. 55°, 60° and 80°, showing that the thienyl group may contribute partially to corrole core conjugation. Rotational fluxionality is further supported by NMR studies provided below.

The measurements of copper corrole cores of those structurally characterized to date are compared in Fig. 4. All examples lack axial substituents, in contrast to the cobalt complexes presented hereafter.

As illustrated in Fig. 4, copper corrole core measurements are similar, irrespective of peripheral substitution and define a Cu sitting between the four nitrogens that are in a distorted square with all Cu–N bonds 1.87–1.89 Å. The short N···N distance in the distorted square is 2.46 Å and the opposing side is 2.83 Å – a difference of ca. 0.4 Å that is accommodated by the sides of ca. 2.70 Å. These geometric similarities suggest differences that lead to dinuclear products as in the *meso*-5,10,15-trispentafluorophenylcorrole may be mainly electronic in nature.

Molecular structures of cobalt corrole compounds number 14 to date in which almost all of these structures have been characterized as a complex containing a central cobalt of formal oxidation state III. There are structural examples in which the cobalt oxidation state has been assigned as IV

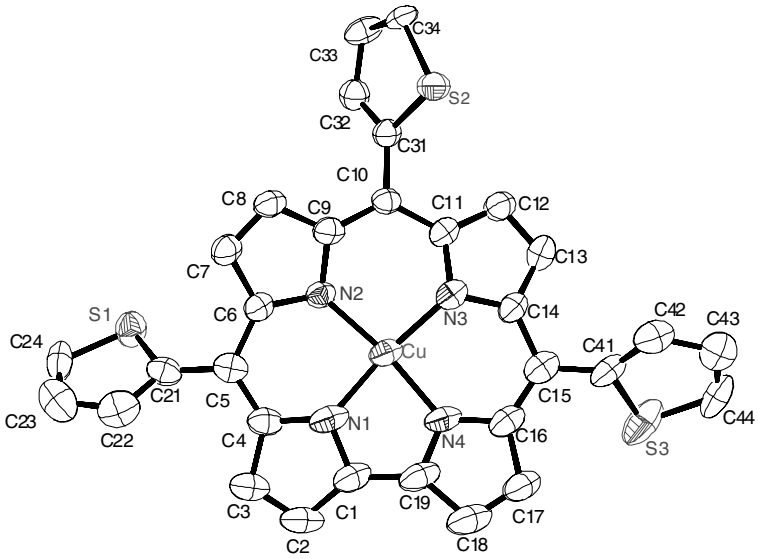

Fig. 2. Molecular structure of Cu(T2TC) (**3**). Thermal ellipsoids are shown at the 50% level. Hydrogen atoms have been removed for clarity.

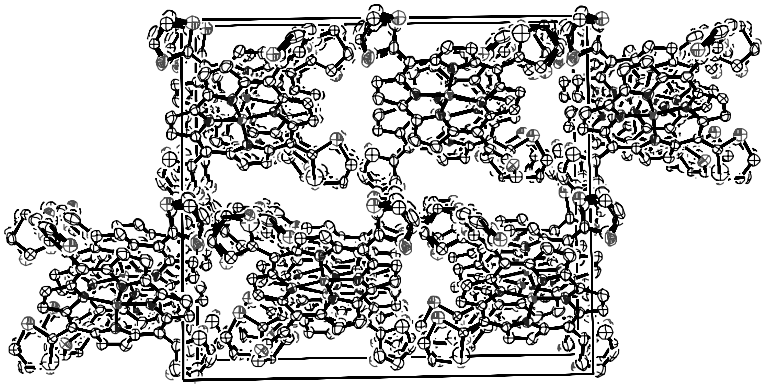

Fig. 3. The crystallographic packing array of Cu(T2TC) (**3**) when looking down the *b*-axis. Both disordered thienyl groups are present and hydrogens are omitted for clarity.

and V [36,37]. Interestingly, the axial pyridine groups in Figs. 5 and 7 are nearly orthogonal to each other. Structures in which orthogonality and near coplanarity have been previously reported [11,38,39].

2.3. NMR spectroscopy

To probe the dynamics of our systems, variable temperature NMR spectra have been obtained for complexes **3** and **4**. Variable temperature stack plotted ^{1}H NMR data are provided below, obtained between the temperatures of −50 and 60 °C (Figs. 9 and 10). Noteworthy is the difference in spectral signal broadening over this range. This is thought to be due exclusively to the different rotational conformations in the metallocorroles of the thienyl groups whose rotations are on the time scale of NMR at the temperature of the studies, not due to the change in electronics of the Cu core [6]. ^{1}H NMR spectra, below room temperature feature broad signals. This same shifting is apparent in the free corrole base. Upon complexation, there is a slight degree of up-field shifting with respect to metal free corroles. High temperature ^{1}H NMR spectra of the Cu complexes appear more resolved [40]. These data indicate that the diamagnetic square planar d^8 complexes with low spin Cu(III) ions coordinated by closed-shell corroles. Our studies in $CDCl_3$ solvent precluded examining beyond these minimum and maximum temperatures.

In the cobalt complex, the proton signals of the *trans* axial pyridines in a 2:4:4 ratio are all up-field shifted perhaps due to the formation of diamagnetic current-effect of the corroles in the complexes [11]. With the common $-C_6F_5$ substituent, there is greater bulk and greater symmetry which does give rise to broadening, but the proton spectrum of the species is simplified.

In addition to these obtaining NMR, all compounds were characterized by UV–vis spectra. Porphyrinoids and corresponding metal complexes give rise to a Soret band, the strong ligand based π–π^* electron transition. These bands for compounds **1**–**6** appear in Table 4. The sulfur atom that is changed from the α-(2-thienyl) to the β-(3-thi-

Table 3
Crystal data for Cu(T2TC) (**3**), Co(T2TC)$(Py)_2 \cdot C_6H_6$ (**5**), and Co(T3TC)$(Py)_2$ (**6**)

Compound	Cu(T2TC) (**3**)	Co(T2TC)$(Py)_2 \cdot C_6H_6$ (**5**)	Co(T3TC)$(Py)_2$ (**6**)
CCDC deposit no.	273811	273812	277370
Empirical formula	$C_{31}H_{17}CuN_4S_3$	$C_{47}H_{27}CoN_6S_3$	$C_{41}H_{27}CoN_6S_3$
Formula weight	605.21	830.86	758.80
Temperature (K)	293(2)	293(2)	293(2)
Radiation (λ), Å	0.71073	0.71073	0.71073
Crystal system	monoclinic	triclinic	triclinic
Space group	$C2/c$	$P\bar{1}$	$P\bar{1}$
a (Å)	10.374(13)	11.6509(13)	9.705(4)
b (Å)	23.21(3)	12.4878(14)	11.745(5)
c (Å)	20.625(17)	15.4676(18)	16.401(6)
α (°)	90	98.237(2)	101.298(7)
β (°)	95.53(5)	105.613(2)	95.059(7)
γ (°)	90	106.376(2)	112.872(7)
V (Å^3)	4942(9)	2020.1(4)	1661.0(11)
Z	8	2	2
Calculated density (Mg/m^3)	1.627	1.366	1.517
Absorption coefficient (mm^{-1})	1.169	0.622	0.748
F(000)	2464	852	780
θ Range for data collection (°)	1.75–28.02	1.41–28.04	1.29–28.06
Limiting indices	$-12 \leqslant h \leqslant 13$, $-24 \leqslant k \leqslant 30$, $-26 \leqslant l \leqslant 26$	$-15 \leqslant h \leqslant 15$, $-15 \leqslant k \leqslant 16$, $-19 \leqslant l \leqslant 19$	$-12 \leqslant h \leqslant 12$, $-14 \leqslant k \leqslant 15$, $-21 \leqslant l \leqslant 20$
Reflections collected/unique	14655/5658 [$R_{int} = 0.0774$]	22713/8931 [$R_{int} = 0.0987$]	19070/7487 [$R_{int} = 0.0715$]
Completeness to theta	94.4%	91.1%	92.8%
Absorption correction	SADABS	SADABS	SADABS
Refinement method	full-matrix least-squares on F^2	full-matrix least-squares on F^2	full-matrix least-squares on F^2
Data/restraints/parameters	5658/85/463	8931/42/503	7487/60/571
Goodness-of-fit on F^2	1.027	1.017	1.008
Final R indices [$I > 2\sigma(I)$]	$R_1 = 0.0608$, $wR_2 = 0.1088$	$R_1 = 0.0793$, $wR_2 = 0.1818$	$R_1 = 0.0528$, $wR_2 = 0.1095$
R indices (all data)	$R_1 = 0.1584$, $wR_2 = 0.1280$	$R_1 = 0.1998$, $wR_2 = 0.2138$	$R_1 = 0.1169$, $wR_2 = 0.1314$

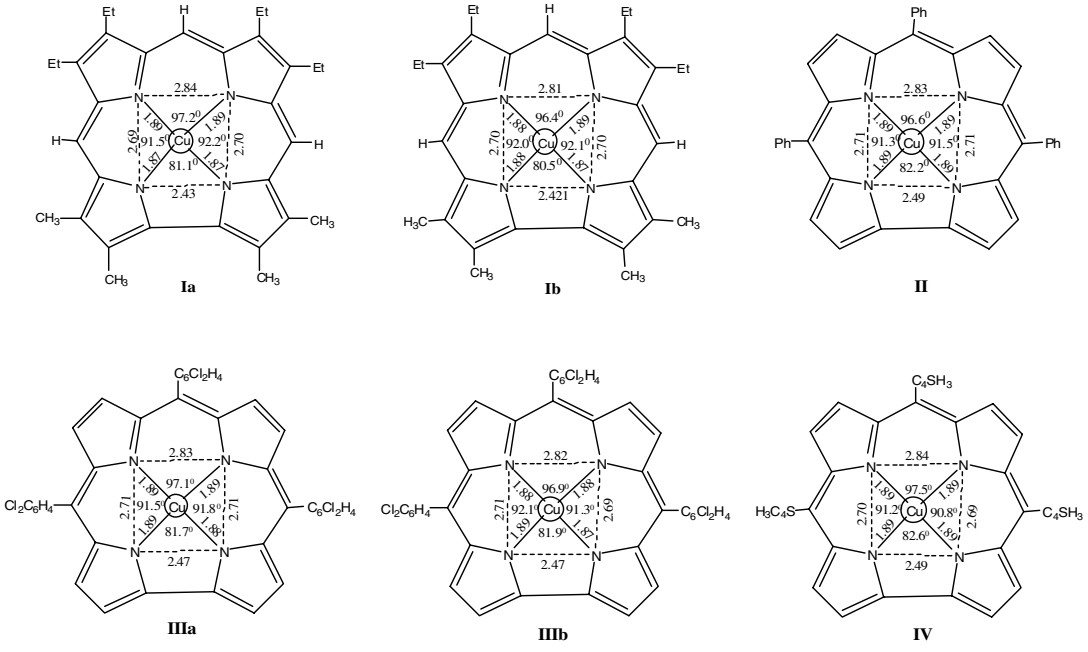

Fig. 4. Comparison of the cores of known Cu corrole complexes. **Ia**, **Ib** [36]; **II**, [29]; **IIIa,b**; [8]; **IV**, this work.

enyl) position in the *meso* substitution gives rise to a band that is always comparatively higher in energy. When the cobalt complex is in solution with excess pyridine, it too becomes blue shifted. This suggests a mono-pyridine derivative forms [11]. A small but measurable difference of 9 nm is detected towards higher energy from 425 in **1** to 416 in **2**.

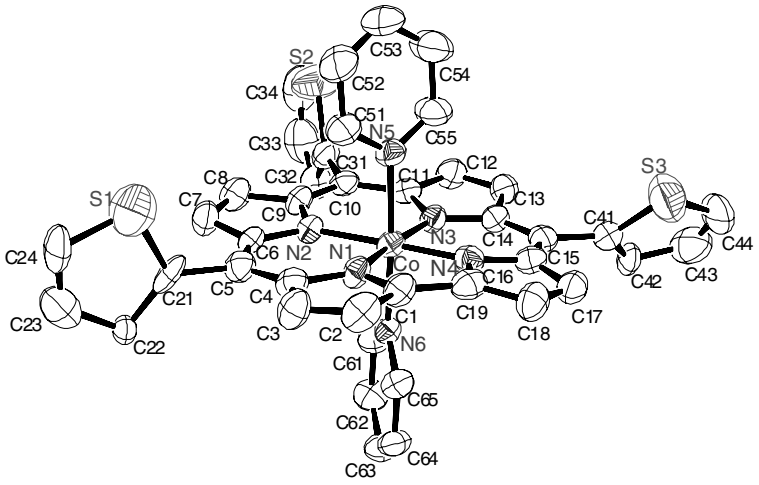

Fig. 5. Molecular structure of Co(T2TC)(Py)$_2$ (**5**). Thermal ellipsoids are shown at the 50% level. Hydrogen atoms and the benzene molecule are omitted for clarity.

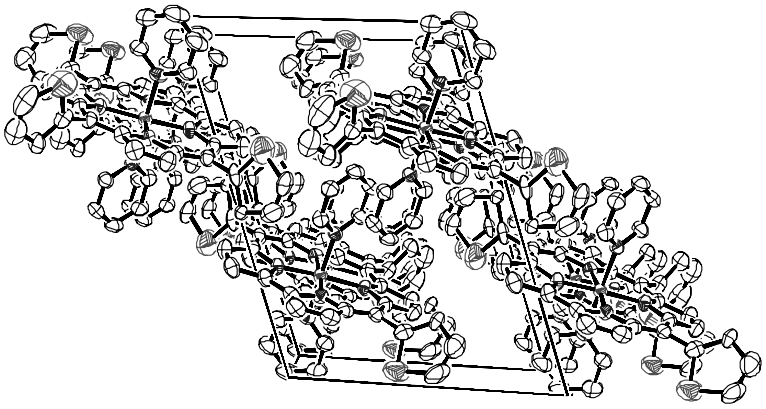

Fig. 6. The crystallographic packing array of Co(T2TC)(Py)$_2$ (**5**) when looking down the *b*-axis. Hydrogens are omitted for clarity.

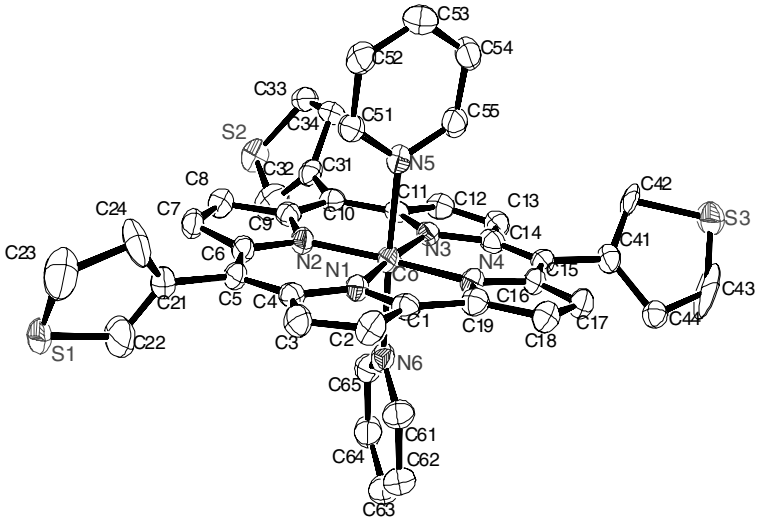

Fig. 7. Molecular structure of Co(T3TC)(Py)$_2$ (**6**). Thermal ellipsoids are shown at the 50% level. Hydrogen atoms have been removed for clarity.

The values for the porphyrins exhibit the same trend at H_2(T2TP): 426 (5.59) and H_2(T3TP) 421 (5.76) [30]. Upon copper complexation, the bands are red shifted keeping an isomeric separation of 21 nm; the corresponding porphyrin system yields a separation of 3 nm [30]. The cobalt metallocorrole isomeric difference is 8 nm.

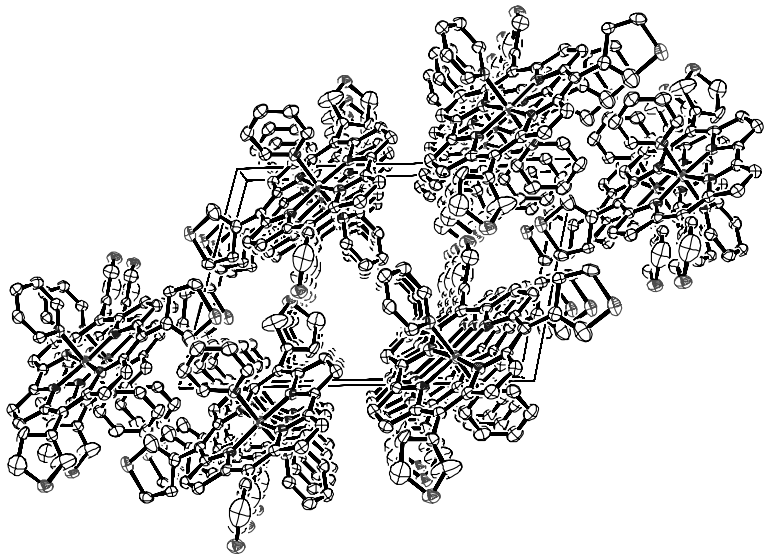

Fig. 8. The crystallographic packing array of Co(T3TC)$(Py)_2$ (**6**) when looking down the *b*-axis. Hydrogens are omitted for clarity. Thermal ellipsoids are shown at the 50% level.

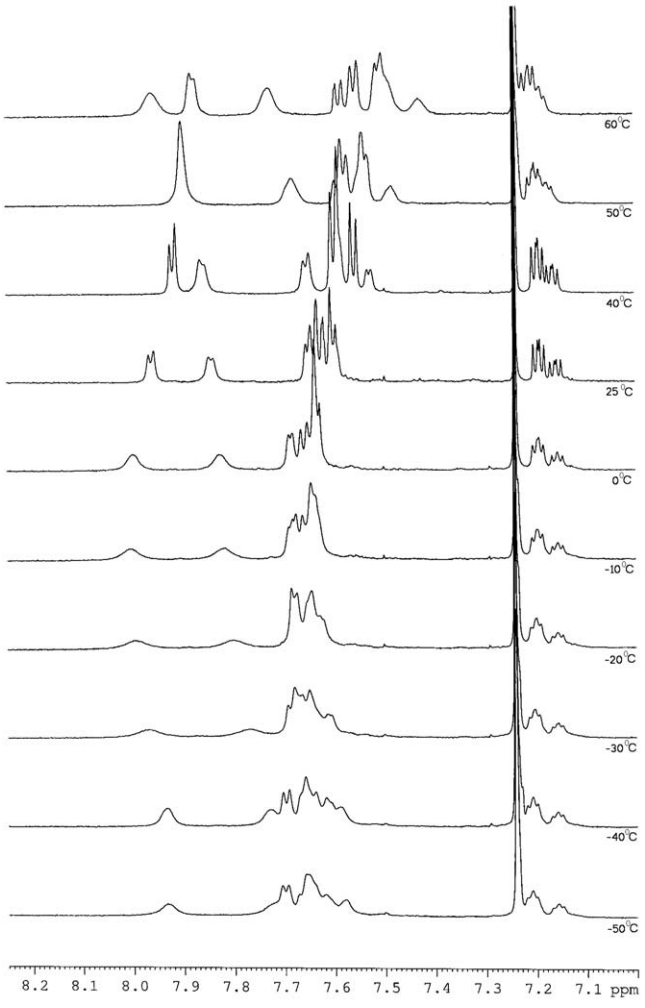

Fig. 9. Aromatic region (7–8 ppm range) of the ^{1}H NMR spectra for Cu(T2TC) (**3**) from −50 °C (bottom) to 60 °C (top).

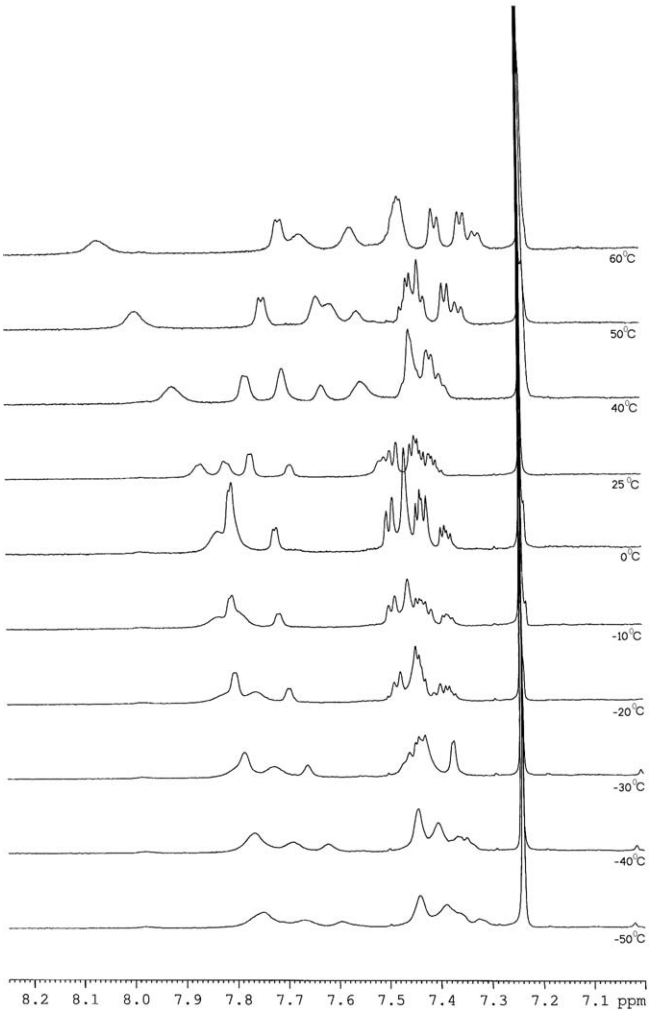

Fig. 10. Aromatic region (7–8 ppm range) of the ^{1}H NMR spectra for Cu(T3TC) (**4**) from −50 °C (bottom) to 60 °C (top).

Table 4
Soret band assignments for corroles and metallocorroles

Compound	λ_{max} (nm), (log ε/($M^{-1}.cm^{-1}$))
H_3(T2TC) (**1**)	425 (5.17)
H_3(T3TC) (**2**)	416 (4.78)
Cu(T2TC) (**3**)	442 (4.82)
Cu(T3TC) (**5**)	421 (5.05)
Co(T2TC)$(Py)_2$ (**4**)	446 (4.96)[a]
	411 (4.97)[b]
Co(T3TC)$(Py)_2$ (**6**)	438 (4.85)[a]
	397 (4.99)[b]

[a] In the presence of excess pyridine.
[b] In the absence of excess pyridine.

2.4. Mass spectrometry

Further data have been obtained to support the enhanced stability of metallocorrole compounds **3**, **4**, **5** and **6** towards C–C coupling, as compared to the $–C_6F_5$ substituted systems. The mass spectra of the copper isomer complexes **3** and **4** show no degree of C–C dinuclear coupling, and the isolated material for the Co isomers shows small observable peaks by high resolution mass spectrometry (see mass spectra provided in the Supporting Information). The monomers seem markedly more stable at room temperature than the corresponding $–C_6F_5$ systems. The [$(\mathbf{3})_2$-2H] products that these signals suggest were not isolated, but only characterized by mass spectrometry but thought to be the same C–C coupling species as those seen by Gross and coworkers [8]. Compared to the $–C_6F_5$ substituted systems, coordinating solvents for these systems were not required. The cobalt compound was further purified by preparative TLC before performing the cyclic voltammetry studies provided below. Material for these studies was made possible through the recrystallization of cobalt crystals with a DCM and *n*-heptane mixture.

2.5. Electrochemistry

The cyclic voltammograms (CVs) of the 5,10,15-tris(thienyl)corrole ligands (**1** and **2**) and their corresponding complexes (**3**, **4**, **5** and **6**) have been obtained and are presented below. Their redox potentials are also provided (Fig. 11).

The reversible half-wave potentials ($E_{1/2}$) for Cu(T2TC) are −0.57 and 0.27 V. The potential at 0.27 V, compares to the oxidation potential of metal-free corrole [$E_{1/2} = 0.15$ V] and has been assigned to corrole-centered oxidation, while the reduction potential at −0.57 V has been assigned to the metal center. The difference in this redox couple ($E_{1/2(ox)} - E_{1/2(red)}$; 0.84 V) also indicates that the two different centers are involved for reduction and oxidation processes (see Table 5).

$$(T2TC)Cu^{II} \underset{-e^-}{\overset{+e^-}{\rightleftharpoons}} (T2TC)Cu^{III} \underset{+e^-}{\overset{-e^-}{\rightleftharpoons}} (T2TC^{\bullet+})Cu^{III} \quad (1)$$

The one-electron oxidation of the 5,10,15-tris(2-thienyl)corrole ligands (**1**) is similar to that of the 5,10,15-tris(3-thienyl)corrole ligands (**2**). The 5,10,15-tris(2-thienyl)corrole ligand (**1**) and its metal complexes (**3** and **5**) have more positive redox potentials than those of the corresponding 3-thienyl ligand (**2**) and its metal complexes (**4** and **6**) because of the greater electron-withdrawing power of 5,10,15-tris(2-thienyl)corrole ligands. This is further supported by a consideration of Hammett and Modified Swain-Lupton Constants (Table 6). Sulfur oxidation has not fully been ruled out in this case. Lastly, these systems are not directly analogous to the corresponding tetrathienyl porphyrin derivatives in that the porphyrin systems undergo two oxidations and two reductions each [30].

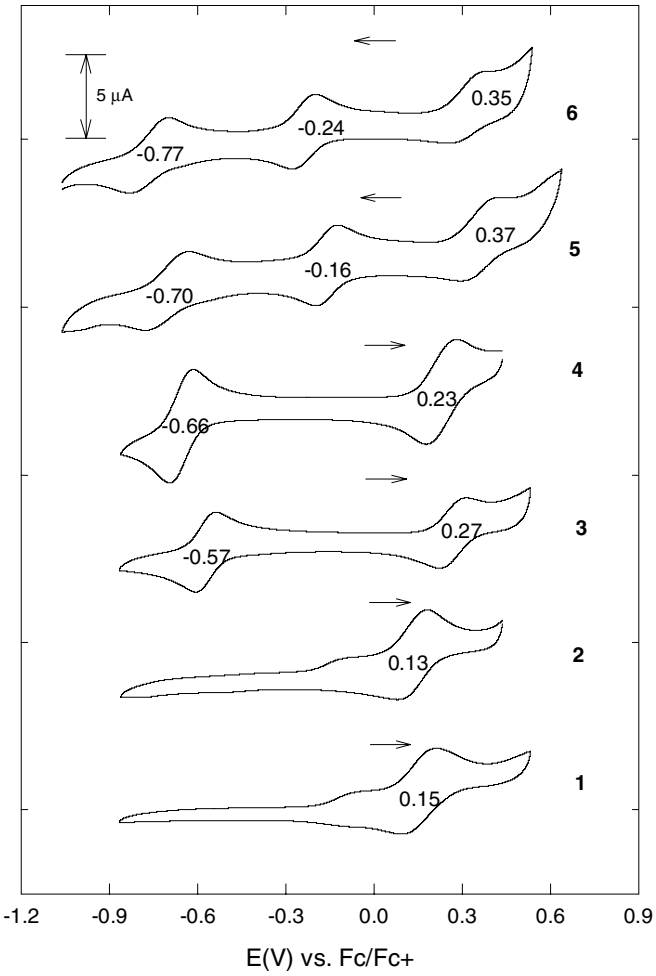

Fig. 11. The cyclic voltammograms of 1 mM 5,10,15-tris(thienyl)corrole ligands (**1** and **2**), 1 mM copper(III) 5,10,15-tris(thienyl)corrole (**3** and **4**), and 1 mM cobalt(III) 5,10,15-tris(thienyl)corrole (**5** and **6**) in benzonitrile solution, 0.1 M TBAP at a scan rate of 100 mV/s (second scans are provided only). $E_{1/2}$ (V) values are provided for each species.

As compared with the copper corroles, the species Co(T2TC)$(py)_2$ (**5**) and Co(T3TC)$(py)_2$ (**6**) have two reduction steps (Fig. 11). This is in contrast to the previously reported Co(tpfc)PPh_3 derivative which exhibits an irreversible reduction process [11]. Co(tpfc)PPh_3 loses a PPh_3 group during the reduction process and then changes to a bis-pyridine coordinated complex. In the case of **5** and **6**, there is an absence of phosphine, and there is excess pyridine; thus, the pyridines present at the outset of the

Table 5
Half-wave potentials ($E_{1/2}$, vs. SCE or Fc/Fc^+) of known copper corrole compounds[a]

Compounds	Oxidation (V) vs.		Reduction (V) vs.		Solvent	Reference
	SCE	Fc/Fc^+	SCE	Fc/Fc^+		
$(T2TC)Cu^{III}$		0.27		−0.57	C_6H_5CN	this work
$(T3TC)Cu^{III}$		0.23		−0.66	C_6H_5CN	this work
$[(TPC)Cu^{III}]$	0.76	0.45[b]	−0.20	−0.51[b]	CH_2Cl_2	[28]
$[(TPFC)Cu^{III}]$	1.13	0.82[b]	0.19	−0.16[b]	CH_2Cl_2	[28]
	1.01		0.22		C_6H_5CN	[8]
$[(TDCC)Cu^{III}]$		0.92		0.06	C_6H_5CN	[8]
$[\{T(p\text{-}CH_3\text{-}P)C\}Cu^{III}]$	0.70	0.39[b]	−0.23	−0.54[b]	CH_2Cl_2	[28]
$[\{T(p\text{-}OCH_3\text{-}P)C\}Cu^{III}]$	0.65	0.34[b]	−0.24	−0.55[b]	CH_2Cl_2	[28]
$[\{T(p\text{-}CF_3\text{-}P)C\}Cu^{III}]$	0.89	0.58[b]	−0.08	−0.39[b]	CH_2Cl_2	[28]

SCE values are provided and have been converted into Fc/Fc^+ values where possible.
[a] TPC = 5,10,15-triphenylcorrole; TPFC = 5,10,15-tris(pentafluorophenyl)corrole; TDCC = 5,10,15-tris(2,6-dichlorophenyl)corrole.
[b] Literature values are reported as V vs. SCE (CH_2Cl_2, 0.1 M TBAP) but have been converted to V vs. Fc/Fc^+ using a related value for the estimated standard potential [$E_{1/2}(Fc/Fc^+) = E_{1/2}(SCE) - 0.31$ V] with these conditions: MeCN, 0.2 M $LiClO_4$ which may not be precise for the conditions used herein: CH_2Cl_2, 0.1 M TBAP [41].

Table 6
A comparison of Hammett and Modified Swain-Lupton constants [33]

X	σ_m (σ_3)	σ_p	R^+	R^-	F	R
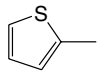	0.09	0.05	-0.56	0.06	0.13	-0.08
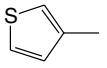	0.03	-0.02	-0.46	0.05	0.08	-0.10
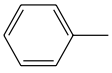	0.06	-0.01	-0.30	-0.10	0.12	-0.13
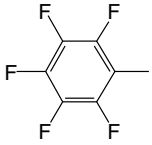	0.26	0.27	-0.09	0.11	0.27	0.00
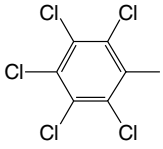	0.25	0.24			0.27	-0.03
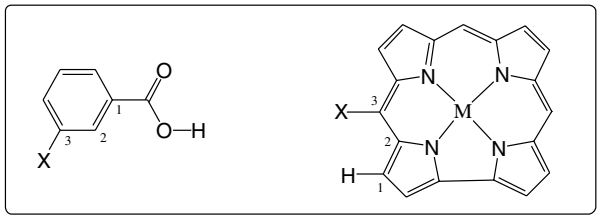						

voltammetric measurement are believed to be retained throughout the course of the experiment. As compared with the copper corrole complexes (**3** and **4**), the cobalt corrole complexes (**5** and **6**) have a more positive oxidation and more negative metal-centered reduction. That means corrole-centered oxidation and metal-centered reduction of cobalt corrole complexes is more difficult than their corresponding copper corrole complexes.

Firstly, *meso* substituents in metallocorroles exert a strong influence on the half-wave potential for one-electron oxidation and this potential is shifted from 820 mV to ca. 270 mV, when the *meso* substituents vary from pentafluorophenyl to thienyl groups. This large decrease in potential shift ca. 550 mV suggests that the removal of an electron is from the corrole "HOMO" [28]. It is easier for thienyl-substituted corroles to be oxidized than the pentaflurophenylphenyl analogs (Table 5) [28].

C–C bond coupling of metallocorroles through the β-carbon in solution has been considered an electronic effect when comparing like tris-*meso*-substituted metallocorroles. Again we see less evidence for corrole oxidation in these thienyl-substituted systems than for tris-pentafluoro derivatives. Thus, Hammett parameters for the various substituents can be discussed. The values for both 2- and 3-thienyl systems are quite similar and can be discussed in connection to electrochemical differences. The Hammett constants (σ) for pentafluorophenyl (pfp)/pentachlorophenyl (pcp) groups are higher than that of 2-thienyl/3-thienyl groups in terms of the ionizations of benzoic acid and *meta*-substituted benzoic acid. Furthermore the electronic effects, i.e. field effects (F) and resonance effects (R) of pfp and pcp substituents are higher than those of both thienyl substituents. By comparing electronic effects with metallocorrole, pfp/pcp groups at the 3-position are more electron withdrawing than the thienyl groups. The 2,6-dichlorophenyl group, though of greater bulk than the thienyl groups, has a greater electron withdrawing effect. C–C coupling is prominent for electron withdrawing substituents at the *meso* positions of metallocorroles but is not necessarily due to the bulkiness of the groups.

3. Conclusions

We have reported novel *meso*-substituted thienyl corroles and the respective metallocorroles for copper and

cobalt. These new derivatives allow for the investigation of compounds electrochemically for coordination and thiophene–thiophene coupling to form macromolecular arrays. Cu(T2TC), Co(T2TC)$(Py)_2$ and Co(T3TC)$(Py)_2$ have been structurally characterized. Dimerization of metallocorroles in solution depends on the electronic effects of the substituents at *meso* positions which are revealed through cyclic voltammetry, NMR and UV–vis spectroscopic data. More electron withdrawing groups tend to give coupling through β-carbons. The bulkiness of the aromatic group is thought to be important. But the thienyl groups are less electron withdrawing than the commonly studied pentafluorophenyl substitutions. Our cyclic voltammetric data support a single oxidation/reduction, devoid of C–C coupling dinuclear products. UV data allow for Soret bands for all ligands and complexes to be measured and indicate red shifting upon metal complexation. One of our strong research motivations involves exploring peroxidase reactivity in related iron systems.

4. Experimental

4.1. General considerations

All solvents and chemicals used in the following synthetic steps were of analytical grade and were used as received: i.e., 2-thiophene carboxyaldehyde, 3-thiophene carboxyaldehyde, pyrrole, $Cu(OAc)_2 \cdot H_2O$, $Co(OAc)_2 \cdot 4H_2O$, pyridine, and C_6H_5CN (Aldrich), dichloromethane, hexane, $MgSO_4$, EtOAc (Merck) and TBAP (Fluka). TBAP was dried overnight under vacuum at 70 °C prior to use. All solvents used for NMR spectral analysis were purchased commercially and were of spectroscopic grade. Infrared spectra were recorded with a Bruker Equinox 55 spectrophotometer and UV–vis spectra were with JASCO V-503 UV–vis spectrometer. A Vario EL III CHNS elemental analyzer was used for microanalysis. High-resolution MALDI mass spectrometry was performed by the staff of the research supporting team at KAIST on a VG AUTOSPEC ULTIMA with a trisector double focusing magnetic sector analyzer at a resolution of 80 000.

^1H spectra were measured in $CDCl_3$ with Bruker Avance 300 and Bruker Avance 400 spectrometers. Variable temperature ^1H NMR spectra were performed in $CDCl_3$ at temperatures between and including −50 and 60 °C. At each temperature, thermal equilibration time was monitored automatically. Spectral signals were calibrated by the protio impurity of the $CDCl_3$ solvent. The synthetic details for the preparation of 5(2-thienyl)dipyrromethane and 5(3-thienyl)dipyrromethane have been reported previously [34,42].

4.2. Physical methods

Cyclic voltammetry was carried out with a BAS 100B (Bioanalytical Systems, Inc.). A three-electrode system was used and consisted of a gold disk working electrode, a platinum wire counter electrode, and a Ag/Ag^+ electrode (MF-2062 kit, Bioanalytical Systems, Inc.) as the reference electrode. The Ag/Ag^+ contained 0.1 M tetrabutylammonium perchlorate (TBAP) and 0.01 M $AgNO_3$ in benzonitrile. In 0.1 M TBAP, the $E_{1/2}$ of the ferrocene/ferrocenium ion couple was taken to be 0.067 V vs. Ag/Ag^+ in benzonitrile. The values in electrochemical experiments are reported versus the ferrocene/ferrocenium ion redox couple.

4.3. X-ray crystallography of Cu(T2TC), Co(T2TC)$(Py)_2$ and Co(T3TC)$(Py)_2$

Crystals of **3**, **5** and **6** suitable for diffraction were grown by slow evaporation of dichloromethane (**3**) and benzene solution, (**5**, **6**), at room temperature. The single-crystal sizes **3**, **5** and **6** were $0.30 \times 0.03 \times 0.20\ mm^3$, $0.50 \times 0.40 \times 0.30\ mm^3$, and $0.3 \times 0.2 \times 0.2\ mm^3$, respectively. Reflection data for **3**, **5**, and **6** were collected on a Bruker 1 K SMART CCD-based diffractometer with graphite-monochromated Mo Kα radiation ($\lambda = 0.7107$ Å). The hemisphere of reflection data was collected as ω scan frames with 0.3°/frame and an exposure time of 5 s/frame under room temperature conditions. Cell parameters were determined and refined by the SMART program [43]. Data reduction was performed using SAINT software [44]. The data were corrected for Lorentz and polarization effects. An empirical absorption correction was applied using the SADABS program [45]. The structures of the compounds were solved by direct methods and refined by full matrix least-squares methods using the SHELXTL program package with anisotropic thermal parameters for all non-hydrogen atoms. Early into the crystallographic solution it was established that each of the three thienyl moieties in compounds **3** and **6** were disordered by ca. 180° rotation about the C_{meso}–$C_{thienyl}$ vector as evidenced by distortions in the atomic thermal parameters upon least-squares refinement. Thiophene fluxionality was evident from VT NMR data provided below, and thus crystallographic disorder was anticipated and has been observed also in the structural solutions for the dipyrromethane precursors [34]. To obtain the molecular structures of **3** and **6** satisfactorily, modeling of this disorder was undertaken and involved creating atomic coordinates for a second thienyl group; both parts were refined to nearly half occupancy. Additionally, the carbon atoms in the benzene solvent molecule of crystallization (in the crystallographic solution for **4**) were refined with the ISOR command in which a given standard deviation is assigned and allows the atomic thermal parameters to approximate isotropic behavior.

4.4. Preparation of 5,10,15-tris(2-thienyl)corrole [H_3(T2TC)]

A sample of 5(2-thienyl)dipyrromethane (1.00 g; 4.38 mmol) and 2-thiophene carboxyaldehyde (0.245 g; 2.19 mmol) were added to 150 mL of a dichloromethane solution of TFA (0.13 mM). The reaction mixture was

standing for 6 h at room temperature. The colour of the solution changed from yellow to pink-red. DDQ (1.0 g, 4.4 mmol) in 50 mL toluene was added during a 10 min period with vigorous stirring. Stirring was continued for an additional 15 min. The reaction mixture was then concentrated and filtered twice through a pad of silica gel using CH_2Cl_2 as the eluent, followed by preparative TLC separation (CH_2Cl_2/hexane 1:1). A broad dark green band was collected as pure corrole (71 mg, 3.0%). *m/z* ($M + H^+$): 545.08 Calc. 545.11 Obs. IR (KBr; cm^{-1}): 3436; 3361 [ν_{N-H}]. ^1H NMR (δ; $CDCl_3$): 9.10 [br, 2H], 8.87 [br, 2H], 8.72 [br, 4H], 7.96 [br, 2H], 7.83 [br, 4H], 7.54 [br, 3H] at 25 °C. 9.10 [br, 2H], 8.73 [br, 2H], 8.46 [br, 4H], 7.91 [br, 4H], 7.86 [br, 1H], 7.81 [br, 1H], 7.58 [br, 2H], 7.52 [br, 1H] at −50 °C. UV–vis: λ_{max} ($\log\varepsilon/(M^{-1}\,cm^{-1})$) 627 nm (4.25); 588 nm (4.29); 425 nm (5.17) [Soret band]; 286 nm (4.43).

4.5. Preparation of 5,10,15-tris(3-thienyl)corrole [H_3(T3TC)]

The synthetic procedure of H_3(T3TC) is similar to that of H_3(T2TC) using 5(3-thienyl)dipyrromethane and 3-thiophene carboxyaldehyde as a replacement of 5(2-thienyl)dipyrromethane and 2-thiophene carboxyaldehyde, respectively. The yield was 83.5 mg (3.5%). *m/z* (M^+): 544.08 (calc); 544.19 (obs). IR (KBr; cm^{-1}): 3436; 3373 (ν_{N-H}). ^1H NMR (δ; $CDCl_3$): 8.95 [br, 2H], 8.82 [br, 2H], 8.64 [br, 2H], 8.48 [br, 2H], 8.20 [br, 2H], 8.17 [br, 2H], 8.09 [br, 2H], 7.82 [br, 2H], 7.76 [s, 1H] at 25 °C. λ_{max} ($\log\varepsilon/(M^{-1}\,cm^{-1})$) 622 nm (3.84); 581 nm (3.82); 416 nm (4.78) [Soret band]; 281 nm (4.18).

4.6. Preparation of Cu(T2TC)

Copper(II) acetate monohydrate (excess) was added to a 5 mL pyridine solution of H_3(T2TC) (**1**) (33 mg, 0.63 mmol). The reaction mixture was stirred for 30 min at room temperature during which the colour of the solution changed from green to reddish-brown. The volatiles were then removed by reduced pressure using a vacuum line. The crude product was then dissolved in a minimum volume of dichloromethane and purified by silica gel column chromatography. A reddish-brown fraction containing Cu(T2TC) was collected by using a dichloromethane–hexane (1:1 v/v) eluant. Yield 33.4 mg. (91%). *m/z* ($M + H^+$): 605.00 (calc); 605.97 (obs). ^1H NMR (δ; $CDCl_3$): 7.95 [br; 2H], 7.88 [d; 2H; $J = 3.7$ Hz], 7.72 [br, 2H]; 7.58 [d; H; $J = 5.1$ Hz]; 7.55 [d; 2H; $J = 4.6$ Hz], 7.50 [d; 4H; $J = 4.2$ Hz], 7.42 [br, H], 7.22–7.17 [m; 3H] at 60 °C. λ_{max} ($\log\varepsilon/(M^{-1}\,cm^{-1})$) 521 nm (3.80); 442 nm (4.82) [Soret band]; 312 nm (3.91); 270 nm (4.20).

4.7. Preparation of Cu(T3TC)

The synthetic procedure reported above for Cu(T2TC) was used to generate Cu(T3TC), in which H_3(T3TC) was used in place of H_3(T2TC). Yield 33 mg. (90%). *m/z* (M^+): 604.00 (calc); 604.09 (obs). ^1H NMR (δ; $CDCl_3$): 8.06 [br; 2H], 7.71 [d; 2H; $J = 3.71$ Hz]; 7.67 [br; 2H], 7.57 [br, 2H], 7.47 [m, 4H], 7.40 [d, $J = 4.7$ Hz, 2H], 7.35 [d, $J = 4.2$ Hz, 2H]; 7.32 [d, $J = 4.3$ Hz, H] at 60 °C. λ_{max} ($\log\varepsilon/(M^{-1}\,cm^{-1})$) 565 nm (3.71); 539 nm (3.98); 421 nm (5.05) [Soret band]; 268 nm (4.53).

4.8. Preparation of Co(T2TC)(Py)$_2$

An approximate threefold excess of $Co(OAc)_2 \cdot 4H_2O$ was added to a hot pyridine solution of H_2(T2TC) (33 mg; 0.06 mmol) and this reaction mixture was refluxed for 1 h. After this time, the reaction mixture was cooled to room temperature and the solvent and volatiles were removed by rotary evaporation. The green crude product was dissolved in a minimum volume of dichloromethane and then isolated by vacuum-filtration. A large volume of diethyl ether was added to the filtrate and a brown precipitate formed after a 30-min period which was then separated by vacuum filtration. The green filtrate was collected and pure crystalline Co(T2TC)$(Py)_2$ was obtained slow diffusion of dichloromethane into *n*-heptane solvent. Yield 40.05 mg. (87%). *m/z* ($M^+ - 2Py$): 599.99 (calc.); 600.98 (obs). ^1H NMR (δ; $CDCl_3$): 9.21 [d, $J = 4.7$ Hz, 2H] 9.1 [d, $J = 4.3$ Hz, 2H], 8.94 [br, 1H], 8.89 [br, 2H], 7.92 [br, 2H], 7.79 [d, $J = 4.7$ Hz, 2H], 7.74 [br, 1H], 7.70 [d, $J = 4.7$ Hz, 2H], 7.49–7.52 [m, 2H], 7.40–7.43 [m, 1H], 6.08 [t, 2H; *para*-H of pyridine], 5.28 [br, 4H; *meta*-H of pyridine], 2.13 [b, 4H; *ortho*-H of pyridine]. λ_{max} ($\log\varepsilon/(M^{-1}\,cm^{-1})$) 629 nm (4.48); 588 nm (4.20); 549 nm (4.04); 446 nm (4.96) [Soret band]; 418 nm (4.72); 314 nm (4.43) (in the presence of excess Py).

4.9. Preparation of Co(T3TC)(Py)$_2$

The synthetic procedure of Co(T3TC) $\cdot$ $(Py)_2$ is similar to that of Co(T2TC)$(Py)_2$ using H_3(T3TC) as a replacement of H_3(T2TC). A yield of 42 mg (91%) was obtained. *m/z* ($M^+ - 2Py$): 599.99 (calc); 600.09 (obs). ^1H NMR (δ, $CDCl_3$ RT): 9.32 [2H]; 9.22 [2H]; 9.11 [2H]; 9.07 [2H]; 8.09 [2H]; 7.92 [3H]; 7.82 [1H]; 7.21–7.27 [m, 3H]; 4.81 [b, 2H; *para*-H of pyridine], 4.39 [b, 4H; *meta*-H of pyridine], 2.54 [b, 4H; *ortho*-H of pyridine]. λ_{max} ($\log\varepsilon/(M^{-1}\,cm^{-1})$) 629 nm (4.49); 584 nm (4.04); 543 nm (3.87); 455 nm (4.78); 438 nm (4.85) [Soret band]; 400 nm (4.57); 309 nm (4.33) (in the presence of excess Py).

5. Supporting information

(i) Cif files of the crystallographic determinations of **3**, **5** and **6**: files CCDC-273811, CCDC-273812, and CCDC-277370 are included. These data are available without cost at www.ccdc.cam.ac.uk/conts/retrieving.html or from the Cambridge Crystallographic Data center (CCDC), 12 Union Road, Cambridge CB2 IEZ, United Kingdom; fax +44(0)1223 336033; e-mail: deposit@ccdc.cam.ac.kr.

(ii) Mass spectrometric data. (iii) Photo of a preparative TLC plate prior to isolation of the purified H3(T3TC) material.

Acknowledgement

DGC gratefully acknowledges financial support from KAIST and the BK 21 Project. YD gratefully acknowledges financial support from the CMDS and the BK 21 Project. J.K. gratefully acknowledges financial support from the BK 21 Project and the MICROS project. Professors Sukbok Chang and Iwan Cho are appreciated for their donations of various chemicals. Hack Soo Shin is gratefully acknowledged for his technical assistance in obtaining ^{13}C and Variable temperature NMR spectra. Teresa Lindstead is thanked for her assistance in depositing our crystallographic data to the CCDC.

References

[1] L. Simkhovich, N. Galili, I. Saltsman, I. Goldberg, Z. Gross, Inorg. Chem. 39 (2000) 2704.
[2] Z. Gross, G. Golubkov, L. Simkhovich, Angew. Chem., Int. Ed. 39 (2000) 4045.
[3] L. Simkhovich, A. Mahammed, I. Goldberg, Z. Gross, Chem.-Eur. J. 7 (2001) 1041.
[4] J. Bendix, H.B. Gray, G. Golubkov, Z. Gross, Chem. Commun. (2000) 1957.
[5] L. Simkhovich, I. Goldberg, Z. Gross, Inorg. Chem. 41 (2002) 5433.
[6] L. Simkhovich, I. Luobeznova, I. Goldberg, Z. Gross, Chem.-Eur. J. 9 (2003) 201.
[7] G. Golubkov, Z. Gross, Angew. Chem., Int. Ed. 42 (2003) 4507.
[8] I. Luobeznova, L. Simkhovich, I. Goldberg, Z. Gross, Eur. J. Inorg. Chem. (2004) 1724.
[9] L. Simkhovich, Z. Gross, J. Inorg. Biochem. 86 (2001) 433.
[10] G. Golubkov, J. Bendix, H.B. Gray, A. Mahammed, I. Goldberg, A.J. DiBilio, Z. Gross, Angew. Chem., Int. Ed. 40 (2001) 2132.
[11] A. Mahammed, I. Giladi, I. Goldberg, Z. Gross, Chem.-Eur. J. 7 (2001) 4259.
[12] L. Simkhovich, P. Iyer, I. Goldberg, Z. Gross, Chem.-Eur. J. 8 (2002) 2595.
[13] E. Vogel, S. Will, A.S. Tilling, L. Neumann, J. Lex, E. Bill, A.X. Trautwein, K. Wieghardt, Angew. Chem. 106 (1994) 771.
[14] Z. Gross, L. Simkhovich, N. Galili, Chem. Commun. (1999) 599.
[15] L. Simkhovich, Z. Gross, Tetrahedron Lett. 42 (2001) 8089.
[16] J. Grodkowski, P. Neta, E. Fujita, A. Mahammed, L. Simkhovich, Z. Gross, J. Phys. Chem. A 106 (2002) 4772.
[17] R.A. Eikey, S.I. Khan, M.M. Abu-Omar, Angew. Chem., Int. Ed. 41 (2002) 3592.
[18] Z. Gross, H.B. Gray, Adv. Synth. & Catalysis 346 (2004) 165.
[19] Z. Gross, N. Galili, L. Simkhovich, Tetrahedron Lett. 40 (1999) 1571.
[20] A. Mahammed, I. Goldberg, Z. Gross, Organic Lett. 3 (2001) 3443.
[21] I. Saltsman, A. Mahammed, I. Goldberg, E. Tkachenko, M. Botoshansky, Z. Gross, J. Am. Chem. Soc. 124 (2002) 7411.
[22] I. Saltsman, I. Goldberg, Z. Gross, Tetrahedron Lett. 44 (2003) 5669.
[23] Z. Gross, N. Galili, I. Saltsman, Angew. Chem., Int. Ed. 38 (1999) 1427.
[24] Z. Gross, J. Biolog. Inorg. Chem. 6 (2001) 733.
[25] B. Andrioletti, E. Rose, J. Chem. Soc.,Perkin Trans. 1 (2002) 715.
[26] D. Aviezer, S. Cotton, M. David, A. Segev, N. Khaselev, N. Galili, Z. Gross, A. Yayon, Cancer Res. 60 (2000) 2973.
[27] A. Mahammed, H.B. Gray, J.J. Weaver, K. Sorasaenee, Z. Gross, Bioconjugate Chem. 15 (2004) 738.
[28] I.H. Wasbotten, T. Wondimagegn, A. Ghosh, J. Am. Chem. Soc. 124 (2002) 8104.
[29] C. Bruckner, P.R. Brinas, J.A.K. Bauer, Inorg. Chem. 42 (2003) 4495.
[30] P. Bhyrappa, P. Bhavana, Chem. Phys. Lett. 349 (2001) 399.
[31] Y. Diskin-Posner, S. Balasubramanian, G.K. Patra, I. Goldberg, Acta Crystallogr., Sect. E E57 (2001) m346.
[32] Z.-F. Li, S.-W. Wang, W.-S. Song, H.-N. Deng, Y.-Q. Wang, Y.-X. Wang, Youji Huaxue 23 (2003) 588.
[33] C. Hansch, A. Leo, R.W. Taft, Chem. Rev. 91 (1991) 165.
[34] N. Maiti, J. Lee, Y. Do, D.G. Churchill, H.S. Shin, J. Chem. Cryst. (2005) 949.
[35] D.T. Gryko, K. Jadach, J. Org. Chem. 66 (2001) 4267.
[36] S. Will, J. Lex, E. Vogel, H. Schmickler, J.-P. Gisselbrecht, C. Haubtmann, M. Bernard, M. Gross, Angew. Chem., Int. Ed. Eng. 36 (1997) 357.
[37] S. Will, J. Lex, E. Vogel, V.A. Adamian, E. Van Caemelbecke, K.M. Kadish, Inorg. Chem. 35 (1996) 5577.
[38] J.-M. Barbe, F. Burdet, E. Espinosa, C.P. Gros, R. Guilard, J. Porph. Phthalocyan. 7 (2003) 365.
[39] R. Guilard, C.P. Gros, F. Bolze, F. Jerome, Z. Ou, J. Shao, J. Fischer, R. Weiss, K.M. Kadish, Inorg. Chem. 40 (2001) 4845.
[40] Y.S. Balazs, I. Saltsman, A. Mahammed, E. Tkachenko, G. Golubkov, J. Levine, Z. Gross, Mag. Res. Chem. 42 (2004) 624.
[41] A.J. Bard, L.R. Faulkner, Electrochemical Methods: Fundamentals and Applications, second ed., John Wiley & Sons, Inc., New York, 2001.
[42] B.J. Littler, M.A. Miller, C.H. Hung, R.W. Wagner, D.F. O'Shea, P.D. Boyle, J.S. Lindsey, J. Org. Chem. 64 (1999) 1391.
[43] SMART, version 5.0, Data Collection Software, Bruker AXS, Inc., Madison, WI, 1998.
[44] SAINT, version 5.0, Data Integraton Software, Bruker AXS Inc., Madison, WI, 1998.
[45] G.M. Sheldrick, SADABS, Program for absorption correction with the Bruker SMART system, Universitat Göttingen, Germany, 1996.